IEEE Photonics Journal
An IEEE Photonics Society Publication

Open Access

All-Fiber Acousto-Optic Tunable Bandpass Filter Based on a Lateral Offset Fiber Splicing Structure

Volume 7, Number 1, February 2015

Hao Zhang
Shouxin Kang
Bo Liu
Hongguang Dong
Yinping Miao

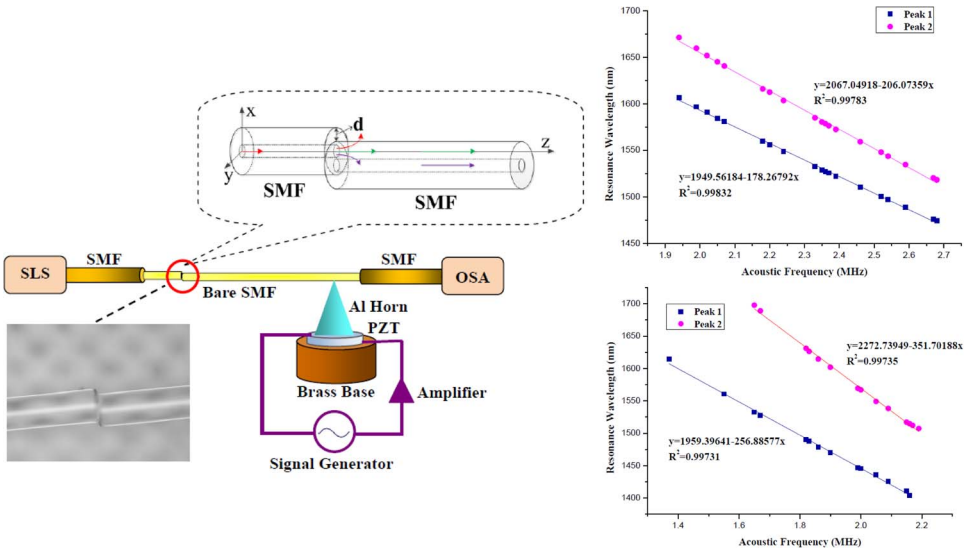

DOI: 10.1109/JPHOT.2014.2387257

All-Fiber Acousto-Optic Tunable Bandpass Filter Based on a Lateral Offset Fiber Splicing Structure

Hao Zhang,[1] Shouxin Kang,[1] Bo Liu,[1] Hongguang Dong,[1] and Yinping Miao[2]

[1]Key Laboratory of Optical Information Science and Technology, Ministry of Education, Institute of Modern Optics, Nankai University, Tianjin 300071, China
[2]Tianjin Key Laboratory of Film Electronic and Communication Device, School of Electronics Information Engineering, Tianjin University of Technology, Tianjin 300384, China

DOI: 10.1109/JPHOT.2014.2387257

Manuscript received November 16, 2014; revised December 17, 2014; accepted December 17, 2014. Date of publication January 1, 2015; date of current version January 26, 2015. This work was supported in part by the National Natural Science Foundation of China under Grant 11274182, Grant 11004110, Grant 61377095, and Grant 11204212; by the 863 National High Technology of China under Grant 2013AA014201; by Tianjin Natural Science Foundation under Grant 13JCZDJC26100; by the National Key Basic Research and Development Program of China under Grant 2010CB327605; by the Fundamental Research Funds for the Central Universities; and by the China Postdoctoral Science Foundation Funded Project under Grant 2012M520024. Corresponding author: H. Zhang (e-mail: haozhang@nankai.edu.cn).

Abstract: An all-fiber acousto-optic tunable bandpass filter has been proposed and experimentally demonstrated by fabricating a lateral offset fiber splicing structure between the lead-in single-mode fiber and acoustic fiber grating. In the presence of acoustic fiber grating that enables the coupling between the antisymmetric cladding modes and symmetric fundamental core mode, the proposed bandpass filter shows a broadband tunable wavelength range up to 152.9 nm with a wavelength tuning sensitivity of −206.07 nm/MHz through adjusting the acoustic frequency. Further experimental results indicate that by using HF acid to etch part of the fiber cladding, the largest tunable bandpass wavelength range could be expanded to 210.2 nm with an improved wavelength tuning sensitivity of −256.89 nm/MHz. Moreover, by adjusting the applied RF signal voltage, a dynamic peak transmission range in a magnitude of ∼10 dB have been experimentally achieved.

Index Terms: Acousto-optic tunable filter (AOTF), optical bandpass filter, acoustic fiber grating, offset fiber splicing.

1. Introduction

The past few decades have witnessed a rapid progress in the field of optical fiber technology, and as one of the key elements for wavelength-division-multiplexing (WDM) telecommunication systems, fiber-optic bandpass filters have attracted considerable research interest. Since Hill *et al.* first attempted to fabricate the long-period grating (LPG) in the late 1970s [1], LPGs have been intensively investigated for applications in optical bandpass filtering owing to their distinguished core-cladding mode resonances, and in recent years, a good variety of delicate LPG-based optical bandpass filter schemes have been proposed. By using a core blocker between two concatenated LPGs, the cladding mode light from the first LPG could be coupled back into the core mode while propagating through the index perturbation region in the second

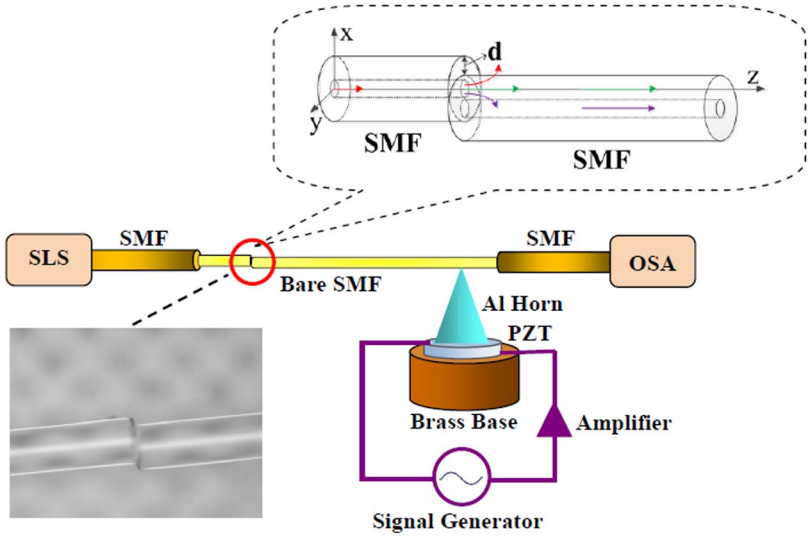

Fig. 1. Schematic diagram of the proposed AOTBF based on offset fiber splicing. Inset shows the micrograph of the offset fiber splicing joint.

grating [2]–[4]. Besides, optical bandpass filtering could be also achieved by exploiting the evanescent field coupling between the LPGs fabricated in two segments of optical fibers placed in parallel [5]. And more recently, by employing an offset fiber splicing structure, the exited cladding mode could be coupled back into the core mode using the LPG fabricated in the lead-out optical fiber [6].

However, in the above optical bandpass filter schemes, complicated and costly grating fabrication procedure based on phase/amplitude mask techniques is normally required and to achieve broadband wavelength tunability is also a quite challenging issue. The most commonly employed thermally controlled wavelength tuning approach will severely limit the wavelength tuning range and has a rather slow filtering response speed [2], [3]. Since Kim *et al.* pioneered work in producing the fiber grating based on flexural acoustic wave modulation in 1986 [7], acoustic fiber gratings have been employed in various tunable fiber-optic bandpass filter schemes owing to their ease of manipulating the mode coupling characteristic through controlling the amplitude and frequency of the electric driving signals for acoustic wave generation. In 2006, Kang *et al.* presented an acousto-optic tunable bandpass filter (AOTBF) based on intermodal coupling in a two-mode fiber [8], and in 2007, the core mode blockers adopted in the aforementioned bandpass filters based on conventional LPGs was introduced to a LPG pair produced by acoustic wave modulation [9].

In this paper, we have proposed and experimentally demonstrated a broadband tunable bandpass filter based on offset fiber splicing between the lead-in single-mode fiber (SMF) and acoustically induced fiber grating. Experimental results indicate that the cladding mode light coupled from the core mode of the lead-in SMF could be re-coupled back into the core mode of output fiber with the assistance of acoustic fiber grating. Owing to the reconfigurable index modulation pattern along the fiber axis, the resonance wavelength, as well as peak transmission, could be tuned by, respectively, adjusting the frequency and voltage of applied electric driving signals. Furthermore, by etching the fiber segment under acoustic wave modulation with HF acid, the acousto-optic coupling efficiency has been greatly enhanced to achieve a broader wavelength tuning range with larger wavelength sensitivity to the applied acoustic frequency.

2. Operation Principle of the Proposed AOTBF

The configuration of our proposed offset-fiber-splicing-based AOTBF is schematically illustrated in Fig. 1. A supercontinuum light source (SLS) is employed to provide a broadband spectrum

ranging from 600 nm to 1700 nm. The lead-in SMF (Corning SMF28-e) is spliced with a segment of bare SMF that is tightly stretched between two fiber clamps with a lateral fiber offset d of about 20 μm. A cone-like Al horn is attached on the top surface of a round PZT plate with primary thickness vibration mode. A signal generator is utilized to provide MHz electrical signals with a peak voltage of 20V that will be amplified by an AC amplifier and then applied onto the PZT plate. In order to effectively apply flexural acoustic wave onto the SMF, the tip of the Al horn is pasted at the bare fiber segment about 10cm away from the offset fiber splicing joint. To avoid the influence of acoustic reflection on the generation of acoustic wave, a cylindrical brass base is attached on the bottom surface of the PZT plate. An optical spectrum analyzer (OSA) is used to monitor the transmission spectrum of the AOTBF in real time.

As the input light from the lead-in fiber enters the output fiber, the fundamental core mode would be coupled into three parts at the fiber offset splicing joint. Some of the input light will be coupled into the cladding leaky mode that quickly dissipates, and a small portion of the light will continue propagating as the fundamental core mode in the output fiber in the presence of a large amount of lateral offset. In the meanwhile, most of the input light will turn into the anti-symmetric cladding LP_{1n} modes [6], [10]. Considering the experimentally adopted side acoustic modulation method that causes an anti-symmetric index modulation over the fiber cross section, the acoustic fiber grating would only support the mode coupling between symmetric LP_{01} core mode and anti-symmetric LP_{1n} cladding modes [11]–[13]. When the LP_{1n} cladding modes excited by the offset fiber splicing joint propagates through the acoustically modulated fiber segment, they will be re-coupled back into the fundamental core mode in the presence of the acoustic fiber grating only at resonance wavelengths determined by the well-known phase matching condition [14]

$$\lambda_{res} = (n_{co} - n_{cl})\Lambda \tag{1}$$

where λ_{res} is the resonance wavelength, and n_{co} and n_{cl} represent the effective refractive indices of the core and cladding modes, respectively. Hence, optical bandpass filtering could be implemented for the resonance wavelengths. Moreover, by adjusting the voltage and frequency of the applied RF signal to respectively manipulate the index modulation strength and acoustic grating pitch, it is convenient to realize broadband tunable bandpass filtering with controllable peak transmission.

3. Experimental Results and Discussion

In order to characterize the wavelength tunability of the proposed AOTBF, we have experimentally observed the transmission spectral evolution for different acoustic frequencies under an applied RF signal voltage of 20 V, as shown in Fig. 2. The peak transmission loss is experimentally measured with respect to the initial transmission spectrum acquired in the case when only a segment of SMF is connected with the SLS and OSA, and to decrease the spectral noise, FFT filtering has been performed to the transmission spectra observed in our experiment. From this figure, it could be seen that two primary peaks, respectively, specified as Peak 1 and Peak 2, are simultaneously present in the transmission spectrum, and the spectral spike around 1700 nm is caused by the spectral noise resulting from the rather low output power of the SLS employed in our experiment for the longer wavelength region. Another issue that should be noted is that since the core mode index of lead-in fiber decreases with the increment of wavelength, the core mode field area would enlarge accordingly, leading to the enhancement of the remnant core mode light that propagates in the output fiber. Therefore, the spectral transmission loss shows a decreasing wavelength dependence. It should be noted that some spectral ripples exist in the transmission spectrum. Experimental observation on the transmission spectra before and after the Al horn is pasted with the bare fiber indicates that these ripples may be caused by the weak interference between the remnant core mode and the cladding modes re-coupled back into the core modes induced by the index perturbation at the point where Al horn tip is pasted. Also, from this figure, it could be seen that as the acoustic frequency increases the transmission peaks exhibit

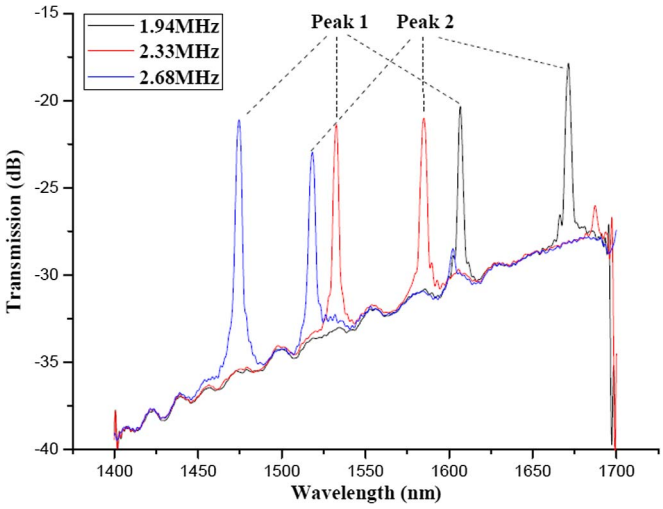

Fig. 2. Transmission spectral evolution of the proposed AOTBF for different acoustic frequencies under an applied RF signal voltage of 20 V.

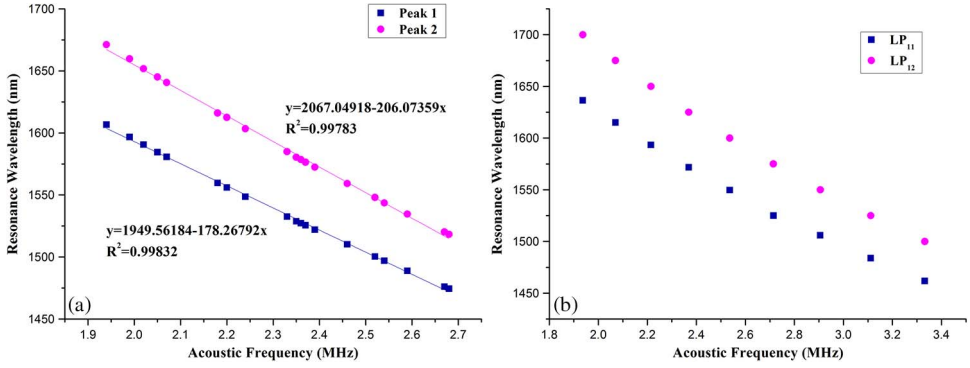

Fig. 3. Resonance wavelength as functions of acoustic frequency for Peak 1 and Peak 2, respectively. (a) Experimental measurement results under an applied RF signal voltage of 20 V. (b) Theoretical calculation results.

considerable blue shift, and this matter has been further investigated through experimental observation on the frequency-dependent spectral evolution. Fig. 3(a) gives the respective acoustic dependences of resonance wavelength for the two transmission peaks under an applied RF voltage of 20 V. It is apparent that as the acoustic frequency increases from 1.94 MHz to 2.68 MHz, both of the two transmission peaks show linear wavelength shift toward shorter wavelength region by about 132.2 nm and 152.9 nm, respectively. In addition, their frequency sensitivities reach -178.27 nm/MHz and -206.07 nm/MHz, respectively. By comparing the acoustic frequency dependences of transmission peak wavelength with the experimental results of our pervious work [15], Peak 1 and Peak 2 should originate from the mode coupling between the fundamental core mode and the two lowest-order LP_{1n} cladding modes. Fig. 3(b) gives our calculated acoustic frequency dependences of the resonance peak wavelength for the mode coupling between fundamental core mode and LP_{11} and LP_{12} cladding modes by using the aforementioned phase matching condition and the following acoustic dispersion relationship describing the acoustic wavelength in terms of the applied acoustic frequency [16]:

$$\Lambda_a = \sqrt{\frac{\pi R c_{ext}}{f_a}} \tag{2}$$

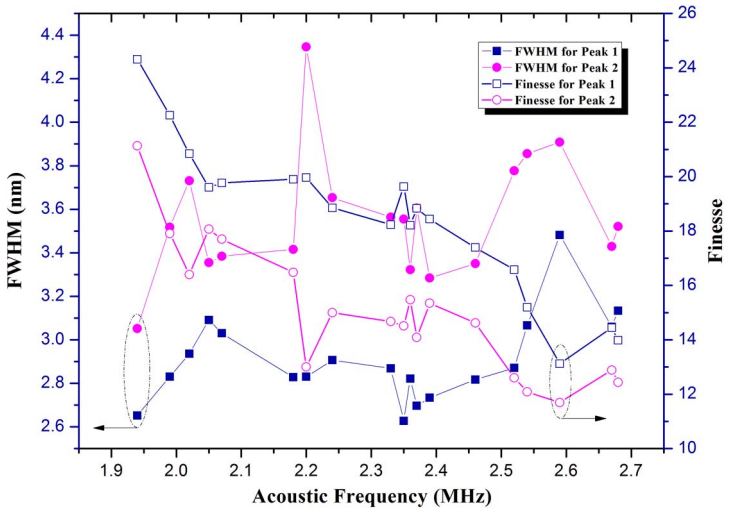

Fig. 4. FWHM and finesse as functions of acoustic frequency for Peak 1 and Peak 2, respectively.

where Λ_a represents the acoustic wavelength that is equal to the acoustic grating pitch, R is the fiber cladding radius, c_{ext} refers to the acoustic wave velocity of the fundamental longitudinal mode in the low-frequency regime, and f_a is the acoustic frequency. From Fig. 3(b), it is clear that as the applied acoustic frequency increases from about 1.94 MHz to 3.33 MHz, the resonance peaks shows some blue shift from 1636.5 nm to 1461.8 nm and 1700 nm to 1500 nm for the LP_{11} and LP_{12} resonance peaks, respectively. The calculated resonance wavelength as functions of applied acoustic frequency are generally in agreement with our experimental results except for some difference due to the deviation of the actual refractive index distribution over the fiber cross section from the parameters adopted in our calculation, and these results confirm that Peak 1 and Peak 2 in the experimentally observed transmission spectrum result from the mode coupling between the fundamental core mode and the two lowest order LP_{1n} cladding modes, respectively.

In order to better characterize the wavelength tunability of our proposed bandpass filter, we have also experimentally measured the full width at half maximum (FWHM) and finesse as functions of applied acoustic frequency for the two resonance peaks in the transmission spectrum, respectively, as shown in Fig. 4, which shows that for an applied acoustic frequency of 1.94 MHz to 2.68 MHz, the FWHMs exhibit slight fluctuations at different acoustic frequencies, which could be attributed to the unequal acoustic amplification ability for different acoustic frequencies of the acoustic horn employed in our experiment. According to the coupled-mode theory, the FWHM $\Delta\lambda$ of an acoustic fiber grating could be approximated as [17]

$$\Delta\lambda \approx \frac{0.8}{L_c}\left[\frac{\partial L_B(\lambda_a)}{\partial\lambda}\right]^{-1}[L_B(\lambda_a)]^2 \tag{3}$$

where L_c is the coupling length, L_B refers to the beat length between the two modes participating in the mode coupling process, and λ_a represents the resonance peak wavelength, respectively. As highly efficient mode resonance occurs, $L_c \approx (\pi/2\kappa_a)$. Here, κ_a is the so-called acousto-optic coupling coefficient determined by [18]

$$\kappa_a = \frac{\pi n_0}{\lambda_a}\sqrt{\frac{\varepsilon_0}{\mu_0}}\iint_A \Psi_1(r,\theta)\Delta n(r,\theta)\Psi_2(r,\theta)rdrd\theta \tag{4}$$

where μ_0 and ε_0 are permeability and dielectric constants in vacuum, respectively; n_0 is effective refractive index of the optical fiber; $\Psi_1(r,\theta)$ and $\Psi_2(r,\theta)$ are electric field distribution of the core and cladding modes, respectively; and $\Delta n(r,\theta)$ is refractive index perturbation induced by

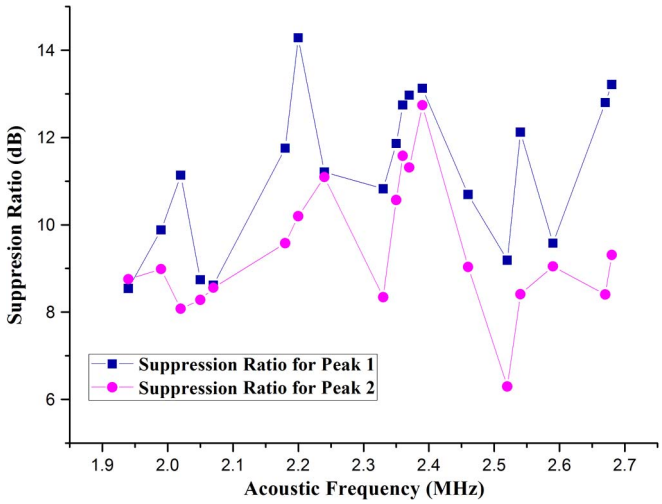

Fig. 5. Suppression ratio as functions of acoustic frequency for Peak 1 and Peak 2, respectively.

the acoustic wave modulation. According to (4), the acousto-optic coupling efficiency is determined by the electric field distribution over the fiber cross section and the acoustically induced refractive index modulation. Since the acoustic amplification ability of the Al-based acoustic horn employed in our experiment is unequal for different applied acoustic frequencies, the refractive index modulation would be frequency dependent, leading to the variation of the acousto-optic coupling efficiency over a certain acoustic frequency range. Therefore, considering $L_c \approx (\pi/2\kappa_a)$ and (3), the FWHM should exhibit the frequency-dependent variation behavior. Moreover, it could be found that the FWHM of Peak 2 is generally larger than that of Peak 1 while both of these two transmission peaks exhibit similar acoustic frequency dependences, and since finesse is determined by the free spectral range (FSR, namely the wavelength spacing between the two resonance peaks for our case) divided by FWHM, from this figure, we could also find that the filter finesse generally shows inverse acoustic frequency dependences in contrast to those of the FWHM. As an important parameter regarding the filter performances, we have also investigated the acoustic frequency dependences of suppression ratio for these two resonance peaks, respectively, as shown in Fig. 5, from which it is clear that also due to the frequency-dependent acoustic amplification ability of the Al horn, the suppression ratios fluctuate from 8.54 dB to 14.28 dB and 8.08 dB to 12.74 dB for Peak 1 and Peak 2, respectively. By designing the horn geometry and using glass-based acoustic horn with acoustic impedance that better matches the silica-based optical fibers, it is possible to further flatten the suppression ratio over a broad acoustic frequency range.

Besides the frequency-dependent spectral responses, we have also investigated the influence of applied RF voltage on the transmission spectral characteristics of the proposed AOTBF. Fig. 6 shows the transmission spectral evolution for an acoustic frequency of 2.2 MHz as the applied RF signal voltage increases from 0 V to 20 V. It is obvious that with the increment of applied voltage, the peak transmission losses for both of Peak 1 and Peak 2 would decrease accordingly. Fig. 7 gives the voltage dependences of peak transmission loss for these two peaks. It can be seen that for the applied RF signal voltage ranging from 3 V to 20 V, due to the enhancement of index modulation, the peak transmission losses decrease by about 12.44 dB and 9.96 dB for Peak 1 and Peak 2, respectively. It should be noted that the voltage sensitivities of peak transmission loss gradually decrease as the applied voltage increases, which indicates the proximity to the grating over-coupling state, and since the acoustic grating transmission rate P, determined by $P = \sin^2(\kappa_a L_c)$, shows a periodic variation behavior with the change of κ_a [19], by comparing the transmission loss sensitivity to the applied voltage, we could find that Peak 2 reaches its saturation state a bit earlier that Peak 1.

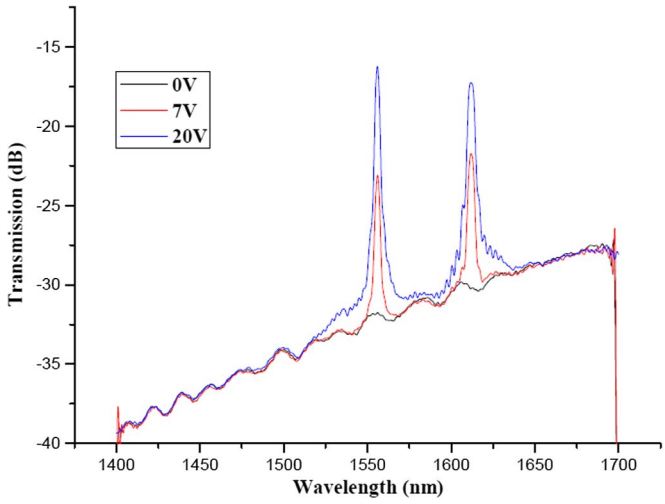

Fig. 6. Transmission spectral evolution of the proposed AOTBF @ 2.2 MHz under different applied RF signal voltages.

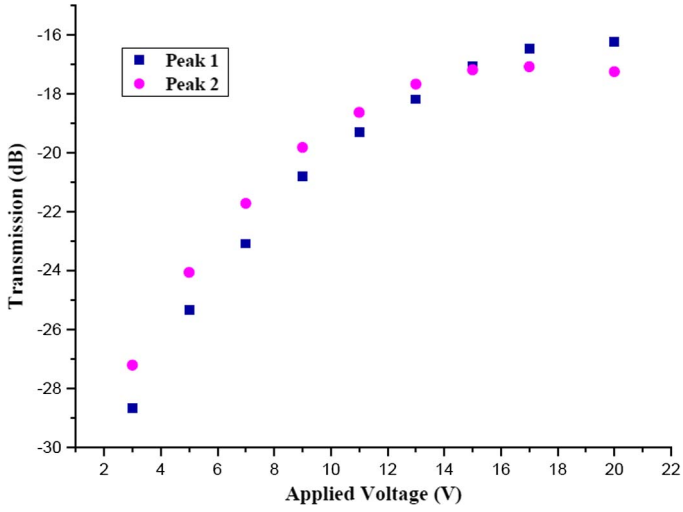

Fig. 7. Peak transmission loss as functions of applied RF signal voltage @ 2.2 MHz for Peak 1 and Peak 2, respectively.

Besides the influence of applied voltage on the peak transmission loss, we have also experimentally investigated the acoustic frequency dependences of transmission loss for the two resonance peaks, as shown in Fig. 8. From this figure, it is apparent that both of Peak 1 and Peak 2 exhibits similar periodic transmission loss variation behaviors with the increment of acoustic frequency. This phenomenon could be mainly attributed to the frequency-dependent refractive index modulation induced by the frequency-sensitive performances of Al horn employed in our experiment. By specifically designing the horn geometry and utilizing glass acoustic horn that better matches the acoustic impedance of silica-based optical fibers, it is possible to improve the frequency response characteristics of peak transmission loss. Similar acoustic frequency dependences of transmission loss for the two resonance peaks have also been experimentally observed in our later study on the proposed fiber filter with partly etched grating segment by using HF acid.

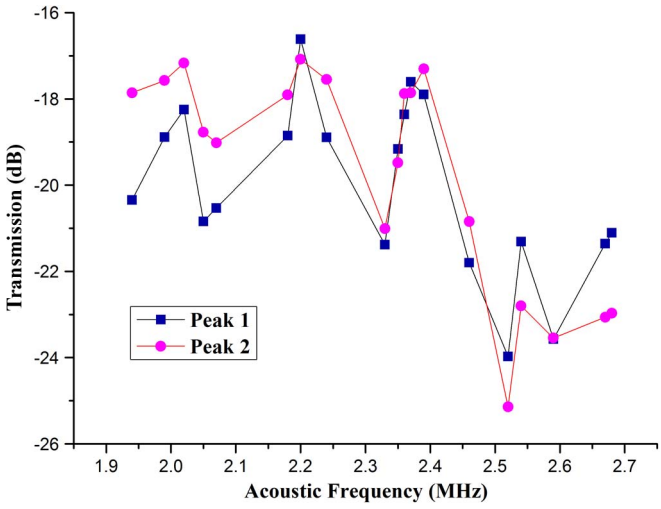

Fig. 8. Transmission loss as functions of acoustic frequency for Peak 1 and Peak 2, respectively.

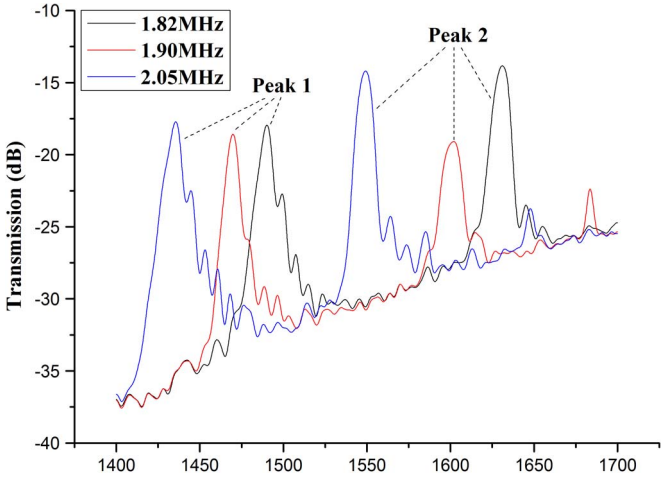

Fig. 9. Typical transmission spectra for different acoustic frequencies under an applied RF signal voltage of 20 V for the AOTBF after HF etching processing.

In order to further enhance the acousto-optic coupling efficiency, 5 cm bare fiber that is about 10 cm away from the offset fiber splicing joint is etched by HF acid until its cladding diameter decreases to about 60 μm. Fig. 9 gives the typical transmission spectra of the proposed AOTBF for different acoustic frequencies under an applied RF signal voltage of 20 V after HF etching processing. Since part of the cladding mode light is re-coupled back into the core mode while propagating through the cladding etched fiber segment, compared with the experimental result shown in Fig. 2, stronger modal interference occurs in the transmission spectrum. Fig. 10(a) shows the experimentally measured resonance wavelength as functions of acoustic frequency of the AOTBF after HF etching processing. According to (2), with the reduction of fiber cladding diameter, lower applied acoustic frequency is required to maintain the acoustic grating pitch. Hence compared with the experimental result shown in Fig. 3(a), it can be seen that the applied acoustic frequency is relatively lower to acquire Peak 1 and Peak 2 within the same experimental wavelength measurement range from 1400 nm to 1700 nm. Moreover, since peak 2 exhibits higher wavelength sensitivity to the applied acoustic frequency, its measurable wavelength

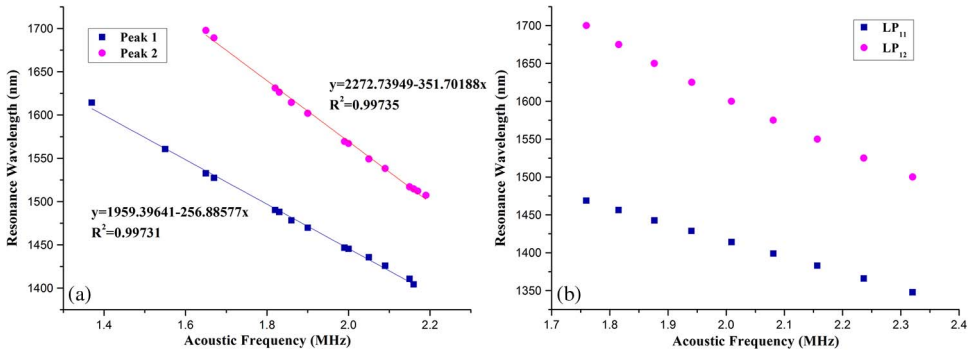

Fig. 10. Resonance wavelength as functions of acoustic frequency for Peak 1 and Peak 2 after HF etching processing, respectively. (a) Experimental measurement results under an applied RF signal voltage of 20 V. (b) Theoretical calculation results.

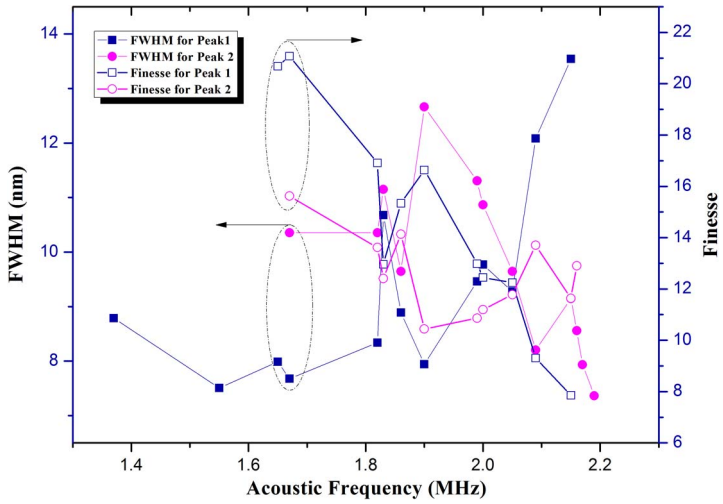

Fig. 11. FHWM and finesse as functions of acoustic frequency for Peak 1 and Peak 2 after HF etching processing, respectively.

tuning range is limited by the wavelength detection up limit of the OSA at 1700 nm. As the acoustic frequency increases from 1.37 MHz to 2.16 MHz, Peak 1 shows a linear blue shift by 210.2 nm while Peak 2 exhibits a linear blue shift by 190.6 nm for an acoustic frequency range from 1.65 MHz to 2.19 MHz. The frequency sensitivities for these two transmission peaks reach about −256.89 nm/MHz and −4351.7 nm/MHz, respectively. These experimental results indicate that by using HF acid to etch part of the fiber cladding, both of the wavelength tuning range as well as frequency sensitivities of resonance wavelength for these two transmission peaks could be greatly improved owing to the enhancement of acousto-optic coupling efficiency, which is in agreement with our previous study on the band-rejection filter based on single acoustic fiber grating [15]. Similar to the results in Fig. 3(b), the theoretical calculation results in Fig. 10(b) indicate that the resonance wavelengths moves toward shorter wavelength region with the increment of acoustic frequency, however, lower acoustic frequency is required to generate resonance peaks within the same wavelength range, which is in accordance with (2) and our experimental observation.

Similar to the study on the bandpass filter before HF etching processing, we have also investigated the FHWM, finesse as well as suppression ratio as functions of the applied acoustic frequency for the two resonance peaks, as shown in Figs. 11 and 12, respectively. Considering

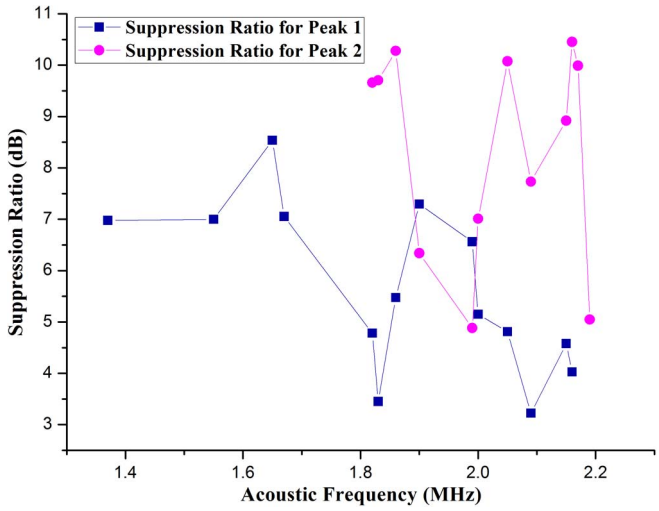

Fig. 12. Suppression ratio as functions of acoustic frequency for Peak 1 and Peak 2 after HF etching processing, respectively.

that not both of the two resonance peaks can be observed throughout the whole experimentally measurement range and some peaks are located quite close to the border of the observable wavelength range, Fig. 11 only gives the FWHM and finesse that could be obtained from the experimentally acquired data. And from this figure, we could see that like the results shown in Fig. 4, the FWHM has also a frequency-dependence change behavior. By comparing the FWHM curves located within the acoustic frequency range where both of the two resonance peaks are present in the transmission spectrum, it could be found that the FWHM of Peak 2 is a bit larger than Peak 1. Moreover, the filter finesse generally shows acoustic frequency dependences inverse to the FWHM. These results are in agreement with our experimental observation for the bandpass filter before HF etching processing. However, by comparing the results in Figs. 4 and 11, it can be found that the FWHM becomes larger for the filter after HF etching processing. This is mainly caused by the improvement of acousto-optic coupling efficiency κ_a defined by (4). As κ_a increases after part of fiber cladding is etched with HF acid, the coupling length L_c will decrease accordingly. According to (3), the FWHM should exhibit broadening to some degree. Also due to the above mentioned reasons, Fig. 12 only gives the experimental measurement results within particular frequency range for these two resonance peaks. And as stronger interference effect takes place when part of the fiber cladding is etched, the suppression ratio is a bit less than that of the filter before HF etching processing. For an acoustic frequency range of 1.37 MHz to 2.16 MHz, the suppression ratio for Peak 1 fluctuates from about 3.22 dB to 8.54 dB. And the suppression ratio of Peak 2 shows some fluctuations from about 4.89 dB to 10.45 dB.

We have also experimentally investigated the dependences of applied RF voltage on transmission spectral characteristics for the AOTBF after HF etching processing, as shown in Fig. 13. Similar to the bandpass filter before HF etching processing, the peak transmission losses for both of Peak 1 and Peak 2 decrease with the increment of applied voltage. And due to the reduction of fiber cladding, notable spectral ripples induced by the modal interference appear in the transmission spectra. Fig. 14 gives the peak transmission losses as functions of applied RF signal voltage for the AOTBF after HF etching processing. It is obvious that for an applied voltage range of 3 V to 20 V, the transmission losses of Peak 1 and Peak 2 decrease by about 10.58 dB and 10.18 dB, respectively, and the voltage sensitivities of transmission losses for both of these transmission peaks generally become lower for higher applied voltage regime, which is in accordance with the experimental results of the AOTBF before the HF etching processing shown in Fig. 7.

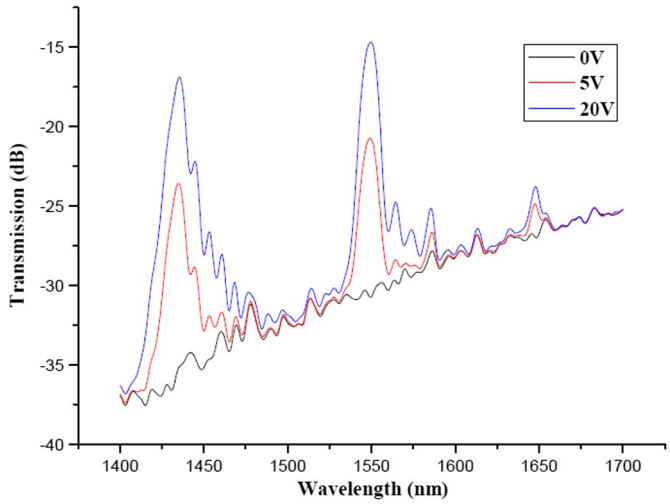

Fig. 13. Transmission spectral evolution @ 2.05 MHz under different applied RF signal voltages for the AOTBF after HF etching processing.

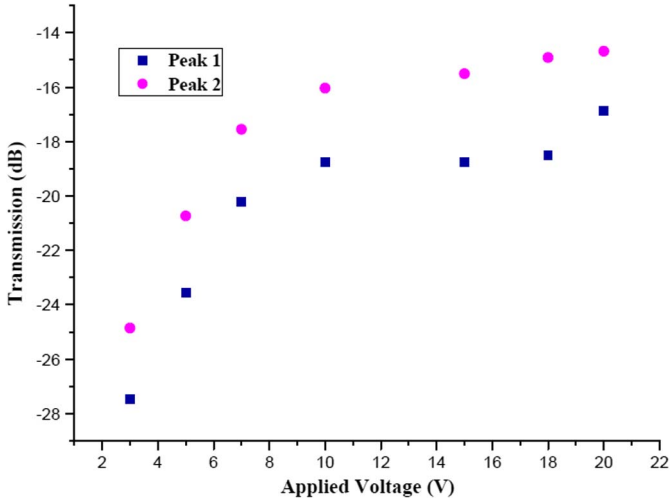

Fig. 14. Peak transmission loss as functions applied RF signal voltage @ 2.05 MHz for the AOTBF after HF etching processing.

4. Conclusion

In summary, we have presented an all-fiber AOTBF based on lateral offset fiber splicing between the lead-in SMF and acoustic fiber grating. Owing to the presence of acoustically induced index modulation along the output fiber axis, part of the anti-symmetric LP_{1n} cladding modes excited from the fundamental core mode of the lead-in SMF could be re-coupled back into the core mode at the resonance wavelengths satisfying the phase matching condition while propagating through the acoustically modulated fiber segment to ultimately be collected at the fiber output port. Experimental results show that the proposed AOTBF could simultaneously support two bandpass channels corresponding to the LP_{11} and LP_{12} cladding mode coupling in the acoustic fiber grating. By adjusting the acoustic frequency, these transmission peaks show wavelength tuning ranges up to 132.2 nm and 152.9 nm with frequency sensitivities of -178.27 nm/MHz and -206.07 nm/MHz, respectively. Moreover, through controlling the applied RF signal voltage, a dynamic peak transmission range in a magnitude of $\sim$10 dB could be achieved. Furthermore,

by etching part of the fiber cladding using HF acid to enhance the acousto-optic coupling efficiency, the wavelength tuning ranges for these two primary transmission peaks could be expanded to 210.2 nm and 190.6 nm, respectively. In addition, their frequency sensitivities have been improved to −256.89 nm/MHz and −351.7 nm/MHz, respectively. The AOTBF presented in this paper possesses several desirable merits such as large wavelength tuning range, high spectral sensitivity to applied acoustic modulation signals, and good spectral re-configurability, which is expected to find potential applications in WDM optical communication, as well as fiber laser systems.

References

[1] K. O. Hill, Y. Fujii, D. C. Johnson, and B. S. Kawasaki, "Photosensitivity in optical fiber waveguides: Application to reflection filter fabrication," *Appl. Phys. Lett.*, vol. 32, no. 10, pp. 647–649, May 1978.

[2] Y. G. Han, S. H. Kim, and S. B. Lee, "Flexibly tunable multichannel filter and bandpass filter based on long-period fiber gratings," *Opt. Exp.*, vol. 12, no. 9, pp. 1902–1907, May 2004.

[3] S. Choi *et al.*, "Broad-band tunable all-fiber bandpass filter based on hollow optical fiber and long-period grating pair," *IEEE Photon. Technol. Lett.*, vol. 17, no. 1, pp. 115–117, Jan. 2005.

[4] H. Sakata, Y. Takata, and S. Suzuki, "Single-channel bandpass filter based on Vernier-aligned long-period fiber gratings," *IEEE Photon. Technol. Lett.*, vol. 19, no. 20, pp. 1661–1663, Oct. 2007.

[5] M. J. Kim, Y. M. Jung, B. H. Kim, W. T. Han, and B. H. Lee, "Ultra-wide bandpass filter based on long-period fiber gratings and the evanescent field coupling between two fibers," *Opt. Exp.*, vol. 15, no. 17, pp. 10855–10862, Aug. 2007.

[6] Q. Zhang, T. Zhu, L. Shi, and M. Liu, "All-fiber bandpass filter based on asymmetrical modes exciting and coupling," *Opt. Commun.*, vol. 286, pp. 161–165, Jan. 2013.

[7] B. Y. Kim, J. N. Blake, H. E. Engan, and H. J. Shaw, "All-fiber acousto-optic frequency shifter," *Opt. Lett.*, vol. 11, no. 6, pp. 389–391, Jun. 1986.

[8] M. S. Kang, H. S. Park, and B. Y. Kim, "Two-mode fiber acoustooptic tunable bandpass filter with zero frequency-shift," *IEEE Photon. Technol. Lett.*, vol. 18, no. 15, pp. 1645–1647, Aug. 2006.

[9] K. J. Lee, D. I. Yeom, and B. Y. Kim, "Narrowband, polarization insensitive all-fiber acousto-optic tunable bandpass filter," *Opt. Exp.*, vol. 15, no. 6, pp. 2987–2992, Mar. 2007.

[10] Z. B. Tian, S. H. Yam, and H. P. Loock, "Single-mode fiber refractive index sensor based on core-offset attenuators," *IEEE Photon. Technol. Lett.*, vol. 20, no. 16, pp. 1387–1389, Aug. 2008.

[11] P. Z. Dashti, Q. Li, C. H. Lin, and H. P. Lee, "Coherent acousto-optic mode coupling in dispersion-compensating fiber by two acoustic gratings with orthogonal vibration directions," *Opt. Lett.*, vol. 28, no. 16, pp. 1403–1405, Aug. 2003.

[12] P. Z. Dashti, Q. Li, and H. P. Lee, "All-fiber narrowband polarization controller based on coherent acousto-optic mode coupling in single-mode fiber," *Opt. Lett.*, vol. 29, no. 20, pp. 2426–2428, Oct. 2004.

[13] P. Z. Dashti, F. Alhassen, and H. P. Lee, "Observation of orbital angular momentum transfer between acoustic and optical vortices in optical fiber," *Phys. Rev. Lett.*, vol. 96, no. 4, Feb. 2006, Art. ID. 043604.

[14] T. Erdogan, "Fiber grating spectra," *J. Lightw. Technol.*, vol. 15, no. 8, pp. 1277–1294, Aug. 1997.

[15] H. Dong, H. Zhang, B. Liu, J. Tao, and L. Liu, "Improvement of coupling efficiency for an acoustooptic tunable filter and its prospects in sensing applications," *Sens. Lett.*, vol. 10, no. 7, pp. 1502–1506, Jul. 2012.

[16] A. Diez, G. Kakatantzas, T. A. Birks, and P. St. J. Russell, "High strain-induced wavelength tunability in tapered fibre acousto-optic filters," *Electron. Lett.*, vol. 36, no. 14, pp. 1187–1188, Jul. 2000.

[17] Y. Jung, S. B. Lee, J. W. Lee, and K. Oh, "Bandwidth control in a hybrid fiber acousto-optic filter," *Opt. Lett.*, vol. 30, no. 1, pp. 84–86, Jan. 2005.

[18] Q. Li *et al.*, "Highly efficient acoustooptic tunable filter based on cladding etched single-mode fiber," *IEEE Photon. Technol. Lett.*, vol. 14, no. 3, pp. 337–339, Mar. 2002.

[19] T. A. Birks, P. S. J. Russell, and D. O. Culverhouse, "The acousto-optic effect in single-mode fiber tapers and couplers," *J. Lightw. Technol.*, vol. 14, no. 11, pp. 2519–2529, Nov. 1996.